the cell-internalizing activities of several hundred monoclonal PTD-PSIF fusions.[8] Therefore, we expect this method to contribute to the identification of mAbs with high cell-internalizing activity (cell-internalizing mAbs) by expressing single-chain antibody Fv (scFv)-PSIF fusion proteins to estimate the cell-internalizing activities of a very large number of antibodies.

Roundabout homolog 4 (Robo4) is a potential tumor angiogenesis marker.[12] Robo4 expression is restricted to areas of in vivo angiogenesis[13,14] and the subpopulation of hematopoietic stem cells localized in the bone marrow.[15] At angiogenic sites, Robo4 is present in the endothelial lining of blood vessels in the developing embryo,[16] placenta,[14] and tumors.[17] We previously confirmed the endothelial cell–specific expression of Robo4 using transgenic mouse lines.[18,19] Robo4 acts as a receptor that modulates vascular endothelial growth factor A (VEGF)–VEGF receptor (VEGFR) signaling.[20-23] Therefore, Robo4 is a potential marker for tumor vascular targeting because angiogenesis is only activated in tumors in the adult,[24] with the exception of some pathological states.[25,26] Another potential tumor angiogenesis marker is VEGFR2, a well-established tumor endothelial marker.[27] The VEGF-VEGFR2 signaling pathway plays a crucial role in angiogenesis, and anti-VEGF mAbs and small molecule inhibitors against VEGFR are approved for various types of cancers.[28] Anti-VEGFR2 mAbs are also used for tumor vascular targeting.[29] Although VEGFR2 is strongly expressed in active angiogenic sites, its expression is also observed in normal tissues.[30] Hypertension and proteinuria are common side effects of anti-VEGF therapy because VEGF-VEGFR signaling is also inhibited in normal tissue, including the kidney, heart, and resistance vessels.[31-33]

Here we applied the PSIF system to search for novel cell-internalizing mAbs from an immune phage antibody library. Application of this method to Robo4 and VEGFR2 led to the successful discovery of anti-Robo4 and anti-VEGFR2 cell-internalizing mAbs, as well as mAbs with low cell-internalizing activity (low-internalizing mAbs) to be used as controls. Comparing mAbs with different cell-internalizing activities revealed that higher cell-internalizing activity enhanced the tumor targeting potency of mAbs. Furthermore, comparative studies with anti-Robo4 and anti-VEGFR2 cell-internalizing mAbs in vivo indicated that Robo4 was superior to VEGFR2 in terms of the therapeutic window. This is the first report demonstrating the benefits of cell-internalizing mAbs in tumor vascular targeting. Further, these findings demonstrate the potential of Robo4 as a target for further development of novel ADCs against tumor blood vasculature.

Materials and methods

Cell culture

MS1 immortalized murine endothelial cells were cultured in Dulbecco's Modified Eagle Medium containing 5% fetal bovine serum 1% antibiotic-antimycotic mixed solution. B16BL6 murine melanoma cells were cultured in minimum essential medium containing 10% fetal bovine serum and 1% antibiotic-antimycotic mixed solution at 37°C. These cells were maintained at 37°C under a humidified 5% CO_2 atmosphere.

B16BL6 tumor-bearing mice

B16BL6 cells (1×10^6 cells/100 μL) were inoculated intracutaneously into 6-week-old female C57BL6 mice (Japan SLC Inc., Shizuoka, Japan) (day 0). Biodistribution was analyzed on the day that the tumor width reached 10 mm. The therapy experiment was started on day 3. As a validation of the model, we confirmed the expressions of VEGFR2 and Robo4 on the tumor endothelium, based on the immunofluorescence against B16BL6 tumor sections.

Antigens

Human VEGFR2 (hVEGFR2) and mouse VEGFR2 (mVEGFR2) were commercial recombinant proteins (Merck Chemicals, Inc., Darmstadt, Germany, or R&D Systems, Inc., Minneapolis, MN). Human Robo4 (hRobo4) and mouse Robo4 (mRobo4) were produced as described previously.[34]

Immune phage antibody libraries

Phage antibody libraries were constructed from the spleen and bone marrow cells of immunized mice as previously described.[35,36] Our phage antibody library comprised single-chain Fv fragment (scFv) fused with pIII phage coat protein. Four rounds of affinity panning were performed against hVEGFR2 and mVEGFR2 for the anti-VEGFR2 immune library, and against hRobo4 and mRobo4 for the anti-Robo4 immune library. Anti-FLAG panning was followed by each panning to concentrate the scFv-displaying phages, as described previously.[36]

ELISA and cytotoxicity assay using TG1 supernatant

Plasmids were extracted from TG1 cells after the fourth panning against mVEGFR2 or mRobo4. These "enriched" scFv gene libraries were cloned into a PSIF-fusion expression vector derived from pCANTAB5E.[8] Monoclonal scFv-PSIF protein was induced in the TG1 supernatant, as previously described.[8] mVEGFR2 or mRobo4 was immobilized on an immunoassay plate and blocked with 4% skim milk in phosphate-buffered saline (PBS) (4% MPBS) at 37°C for 2 hours. TG1 supernatant containing 2% MPBS was reacted with antigens at room temperature for 1 hour. Bound scFv-PSIFs were detected by anti–FLAG-horseradish peroxidase (M2, Sigma-Aldrich Corporation, St. Louis, MO). For the cytotoxicity assay, MS1 cells were seeded on a 96-well plate at 1.0×10^4 cells/well. After incubation at 37°C for 24 hours, TG1 supernatant was diluted in MS1 culture medium, and then added to the MS1 cells. After incubation at 37°C for 24 hours, cell viability was assessed using a WST-8 assay (Dojindo Molecular Technologies, Inc., Kumamoto, Japan). The viability of nontreated MS1 and completely killed MS1 with 1 mM cycloheximide were defined as 100% and 0%, respectively.

Expression and purification of scFv, dscFv, and scFv-PSIF recombinant protein

The isolated scFv gene with 15 amino acids linker (VL-GGGGSGGG GSGGGGS-VH) was cloned into modified pET15b vector, resulting in the scFv fused by FLAG-tag and His×6 tag at the C-terminus. A scFv gene with a 5–amino acid linker (VL-GGGGS-VH) was also cloned into modified pET15b, resulting in a noncovalent scFv dimer (dscFv) fused by FLAG-tag and His×6 tag at the C-terminus. An anti-His scFv gene was also cloned but only a FLAG-tag was fused at the C-terminus. A scFv gene with a 15–amino acid linker was cloned into pYas-PSIF vectors.[37] ScFvs, dscFvs, and scFv-PSIFs were purified from inclusion bodies in *E coli* according to the previously described methods.[37] The binding affinity of each recombinant protein was assessed by surface plasmon resonance using BIAcore3000 (GE Healthcare UK Ltd., Chalfont, United Kingdom).

Expression and purification of IgG recombinant protein

IgG recombinant proteins were expressed using an OptiCHO antibody expression kit (Invitrogen Corporation, Carlsbad, CA) according to the manufacturer's instructions. IgGs were purified from cell culture supernatant with protein G column (GE Healthcare). Eluted fractions were further purified with Superdex 200 column (GE Healthcare). Anti-FLAG[IgG] (anti-FLAG M2 antibody) was purchased from Sigma-Aldrich.

Preparation of IgG-NCS

NCS was kindly provided by Kayaku Co, Ltd., Tokyo, Japan. NCS was thiolated by incubating it with 10 molar excess 2-iminothiolane (Thermo Fisher Scientific Inc., Waltham, MA) for 1 hour at room temperature. IgG recombinant proteins were reacted with 10 molar excess of SPDP

crosslinker (*N*-succinimidyl 3-[2-pyridyldithio]-propionate; Thermo Fisher) for 30 minutes on ice. SPDP-modified IgGs and thiolated NCS were separately purified using NICK columns (GE Healthcare). They were then mixed for 8 hours at room temperature. IgG-NCS were purified with a Superdex 200 column. Modification efficiency was quantified after sodium-dodecyl sulfate-polyacrylamide gel electrophoresis using a Gel DOC EZ system and Image laboratory software (Bio-Rad Laboratories, Inc., Hercules, CA).

Labeling of purified mAbs

For fluorescent labeling, mAbs were labeled using Cy5.5-NHS (GE Healthcare). For ^{125}I labeling, 100 μg mAbs in 0.4 M phosphate buffer were labeled with 0.2 mCi Na^{125}I (PerkinElmer, Inc., Waltham, MA) based on the chloramine-T method.[38] For biotin labeling, mAbs were biotinylated using EZ-Link Sulfo-NHS-Biotin (Thermo Fisher). Each mAb was purified using a NICK desalting column (GE Healthcare).

Flow cytometry

Cy5.5-labeled mAb ($mAb^{Cy5.5}$; 4 μM) was incubated with 5.0×10^5 cells of MS1 cells in 6-well plates for 2 hours at 4°C. After washing three times, the cells were incubated for an additional 0.5 to 8 hours at 37°C. At each time point, cells were collected in 2-mM ethylenediaminetetraacedtic acid/PBS. Bound mAbs were digested using 0.1% trypsin/PBS at 37°C for 20 minutes (trypsinized group) or PBS (nontrypsinized group). Cellular fluorescence was measured by Gallios flow cytometer (Beckman Coulter, Inc., Miami, FL). The ratio of internalization was calculated using the following formula: internalization (%) = {internalized $mAb^{Cy5.5}$}/{total bound $mAb^{Cy5.5}$} × 100 (%) = {(MFI of $mAb)_T$ − (MFI of anti-His $[mAb])_T$}/{(MFI of $mAb)_N$ − (MFI of anti-His$[mAb])_N$} × 100 (%). MFI indicates mean fluorescence intensity. T and N indicate trypsinized and nontrypsinized groups, respectively.

In vivo biodistribution

$dscFvs^{125I}$ (0.2 nmol) was intravenously injected into B16BL6 tumor–bearing mice. At 2 hours and 24 hours after injection, the radioactivity of each organ was counted using the Wizard 2480 γ-ray counter (PerkinElmer). %ID/g tissue was calculated using following formula: %ID/g tissue = (count/g tissue)/(total injected count) × 100 (%). Two individual experiments were combined for the final data (total 11 mice/group).

Immunofluorescence of the tissue sections

B16BL6 tumor–bearing mice were administered 2 nmol of $dscFvs^{Bio}$. At 2 hours after the injection, the tumors, kidneys, and hearts were embedded in optimal cutting temperature compound (Sakura Finetek, Inc., Torrance, CA) and frozen in liquid nitrogen. Thin sections (7 μm) were prepared using a Cryostat CM1850 (Leica Microsystems GmbH, Wetzlar, Germany) and fixed in 4% paraformaldehyde. $DscFvs^{Bio}$ in the sections were stained with streptavidin phycoerythrin conjugate (eBioscience Inc., San Diego, CA) in Dako REAL Antibody Diluent (DAKO Corporation, Carpinteria, CA). CD31+ vascular endothelial cells were stained with rat anti-CD31 antibody (MEC13.3; Becton Dickinson and Company, Franklin Lakes, NJ) in Dako REAL Antibody Diluent and Alexa488 conjugated anti-rat IgG (A11006; Invitrogen). The samples were embedded with Prolong Gold antifade reagent with 4′,6-diamidino-2-phenylindole (Invitrogen) and observed with a fluorescence microscope FSX100 (Olympus Corporation, Tokyo, Japan).

In vivo therapy experiments

Activities of scFv-PSIFs and IgG-NCSes were confirmed by WST-8 assay as described before. B16BL6 cells were inoculated intracutaneously into C57BL6 mice (Japan SLC) on day 0. Mice were intravenously injected with 15 pmol scFv-PSIFs and 10 pmol IgG-NCSs on days 3, 5, 7, 9, and 11 (7 mice/group). The volume of the tumor was calculated according to the following formula: tumor volume (mm^3) = {major axis of tumor (mm)} × {minor axis of tumor (mm)}^{2} × 0.4.

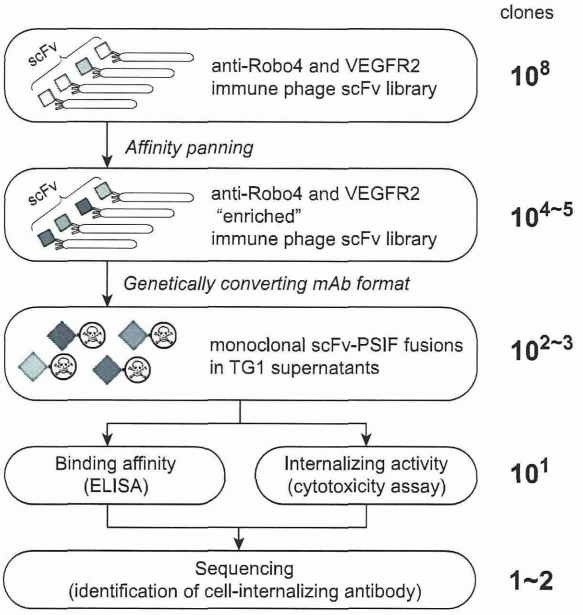

Figure 1. Phage display-based method to search for cell-internalizing mAbs. The phage antibody library was "enriched" by affinity panning against the desired antigens. Plasmids encoding scFvs were collected from TG1 *E coli* strains infected by "enriched" phage libraries. Genes of scFvs were digested out and ligated into a PSIF fusion protein expression vector. These plasmids were then transformed to TG1, and then single colonies were picked up. From these individual colonies, monoclonal scFv-PSIF fusions were induced in TG1 supernatants. Using these fusion proteins, binding affinities and internalizing activities of several hundreds of scFv-PSIFs were easily estimated by ELISA and cytotoxicity assays, respectively. Finally, genes of positive scFvs were collected from TG1, and cell-internalizing scFvs were identified by sequencing. In this report, we used anti-Robo4 and anti-VEGFR2 immune phage scFv libraries as the phage antibody libraries, and mRobo4 and mVEGFR2 as the desired antigens.

Results

High-throughput screening for cell-internalizing mAbs

To identify cell-internalizing mAbs, we applied the phage immune scFv library to high-throughput screening of cell-internalizing molecules based on the PSIF system[8] (Figure 1). Our anti-Robo4 or anti-VEGFR2 phage library comprised approximately 3.0×10^8 or 5.0×10^8 independent scFvs, which was validated by sequence analysis. To assess the qualities of the libraries, affinity panning was performed against each antigen. During the panning, output phages were increased, suggesting that the desired scFvs were enriched in the library (supplemental Figure 1A-B,E-F). After the fourth panning, >40% of monoclonal scFvs showed specific binding in enzyme-linked immunosorbent assay (ELISA) (supplemental Figure 1C-D,G-H).

To validate the efficacy of cell-internalizing mAbs in a mouse model, we selected libraries enriched against murine antigens (mRobo4 and mVEGFR2) and chose MS1 murine endothelial cells for the screening of cell-internalizing mAbs because we confirmed the expressions of both mRobo4 and mVEGFR2 in MS1 cells using reverse transcriptase–polymerase chain reactioin. For the screening, scFv genes obtained after the fourth round of panning were cloned into the PSIF expression vector. Monoclonal scFv-PSIFs were expressed in TG1 supernatants (315 clones per library). For anti-Robo4s, 178 of 315 clones bound to mRobo4 in ELISA and 20 of these 178 binders were cytotoxic against MS1 cells

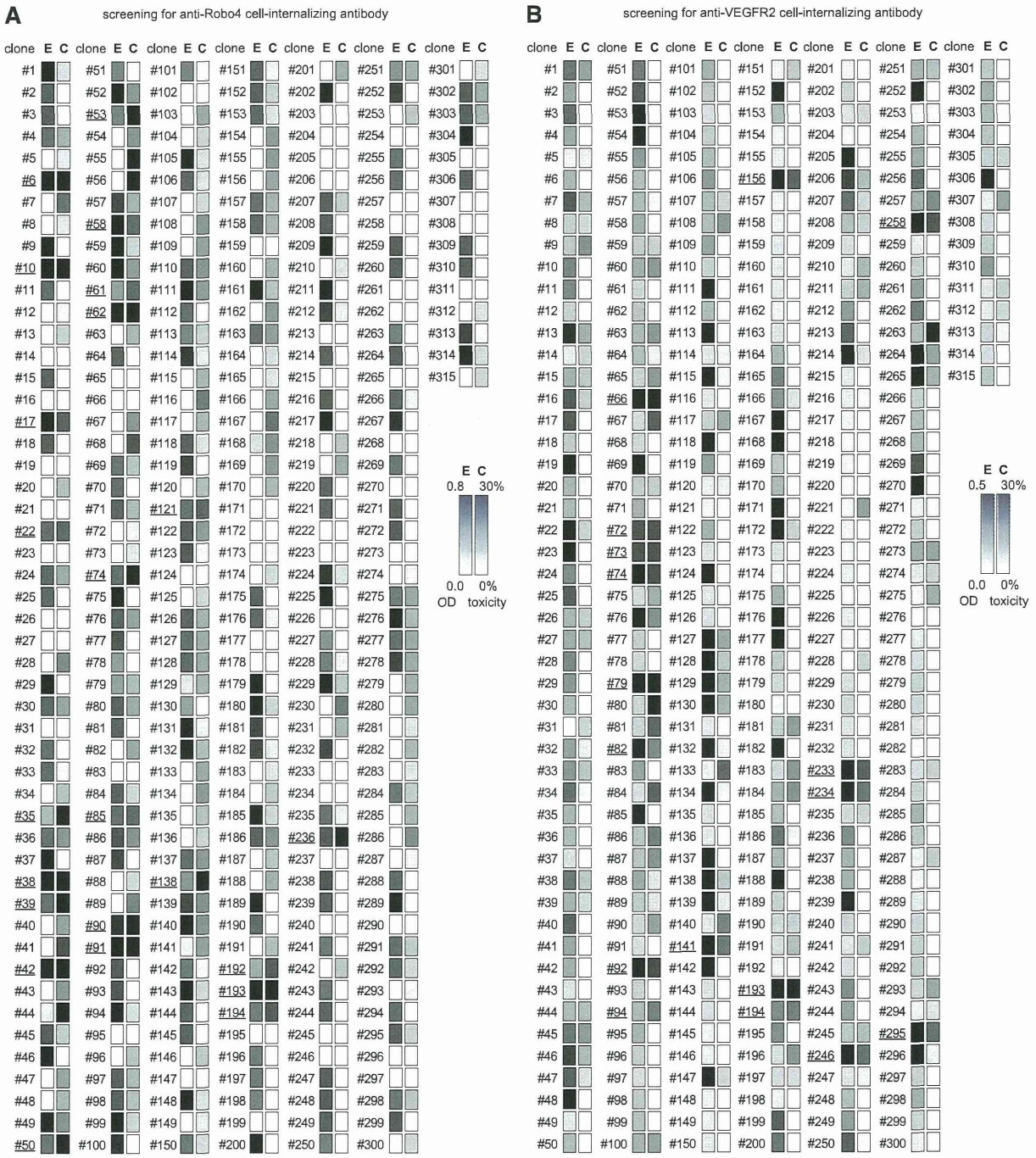

Figure 2. Screening of cell-internalizing mAbs (ELISA and cytotoxicity assay). To screen for cell-internalizing mAbs, 315 clones per antigen were analyzed by ELISA and cytotoxicity assay. (A) Result for Robo4, (B) Result for VEGFR2. Monoclonal scfv-PSIFs were induced in TG1 supernatant. The binding properties and cytotoxicities to MS1 cells were then assessed by an ELISA and WST-8 assay, respectively. E, ELISA results; C, WST-8 assay results. Individual results from ELISA (OD = 0.8 or 0.5~0.0) and WST-8 assay (cytotoxicity = 30%~0%) were mapped in grayscale densities. The 24 candidates against Robo4 and 17 candidates against VEGFR2 are indicated by the underline (ELISA OD ≥0.2 and cytotoxicity ≥20%). After omitting redundant clones by sequencing, 1 cell-internalizing mAb and 2 low-internalizing mAbs against mRobo4, and 2 cell-internalizing mAbs and 14 low-internalizing mAbs against mVEGFR2 were identified.

(Figure 2A). In a similar manner, for anti-VEGFR2s, 156 of 315 clones bound to VEGFR2 and 17 of the 156 binders were positive in the ELISA and cytotoxicity assays (Figure 2B). Sequence analysis to omit redundant clones revealed that these clones comprised 1 anti-Robo4 cell-internalizing mAb, 2 anti-Robo4 low-internalizing mAbs, 2 anti-VEGFR2 cell-internalizing mAbs, and 14 anti-VEGFR2 low-internalizing mAbs. For anti-Robo4s, only one anti-Robo4 cell-internalizing mAb was named "R4-13i" and a low-internalizing mAb with high affinity and low cytotoxicity was named "R4-16." In a similar manner, "V2-05i" and "V2-02" were selected as an anti-VEGFR2 cell-internalizing mAb and a low-internalizing mAb, respectively. After purification of the recombinant proteins, both anti-Robo4 scFvs bound to hRobo4, similar to mRobo4. Conversely, anti-VEGFR2 scFvs bound to

Table 1. Binding kinetics of antibodies in surface plasmon resonance analysis

Antibody	Target	Format	k_a ($M^{-1}s^{-1}$)	k_d (s^{-1})	K_D (M)
R4-13i	mRobo4	scFv	$1.25 \pm 0.36 \times 10^5$	$5.82 \pm 0.95 \times 10^{-4}$	$5.03 \pm 1.95 \times 10^{-9}$
(internalizing)		dscFv	$1.15 \pm 0.34 \times 10^6$	$5.98 \pm 0.61 \times 10^{-4}$	$5.64 \pm 2.21 \times 10^{-10}$
		IgG	$1.14 \pm 0.55 \times 10^6$	$4.19 \pm 1.70 \times 10^{-4}$	$2.22 \pm 0.51 \times 10^{-10}$
		scFv-PSIF	$7.22 \pm 4.31 \times 10^4$	$4.28 \pm 1.60 \times 10^{-3}$	$6.47 \pm 1.61 \times 10^{-8}$
		IgG-NCS	$1.02 \pm 0.15 \times 10^6$	$4.66 \pm 0.86 \times 10^{-4}$	$4.59 \pm 0.74 \times 10^{-10}$
R4-16	mRobo4	scFv	$1.30 \pm 0.33 \times 10^5$	$5.82 \pm 1.50 \times 10^{-4}$	$4.77 \pm 1.96 \times 10^{-9}$
(low-internalizing)		dscFv	$1.12 \pm 0.03 \times 10^6$	$5.91 \pm 1.50 \times 10^{-4}$	$5.31 \pm 1.96 \times 10^{-10}$
		IgG	$1.06 \pm 0.24 \times 10^6$	$3.60 \pm 0.85 \times 10^{-4}$	$2.76 \pm 0.16 \times 10^{-10}$
		scFv-PSIF	$8.90 \pm 1.42 \times 10^4$	$6.10 \pm 2.45 \times 10^{-3}$	$7.24 \pm 3.74 \times 10^{-8}$
		IgG-NCS	$1.07 \pm 0.12 \times 10^6$	$3.93 \pm 0.54 \times 10^{-4}$	$3.72 \pm 0.89 \times 10^{-10}$
V2-05i	mVEGFR2	scFv	$9.66 \pm 3.57 \times 10^4$	$4.40 \pm 0.95 \times 10^{-4}$	$5.13 \pm 2.61 \times 10^{-9}$
(internalizing)		dscFv	$8.75 \pm 2.03 \times 10^5$	$5.59 \pm 2.57 \times 10^{-4}$	$6.16 \pm 1.47 \times 10^{-10}$
		IgG	$1.14 \pm 0.09 \times 10^6$	$3.21 \pm 0.35 \times 10^{-4}$	$2.84 \pm 0.52 \times 10^{-10}$
		scFv-PSIF	$9.57 \pm 0.84 \times 10^4$	$6.51 \pm 1.87 \times 10^{-3}$	$6.94 \pm 2.63 \times 10^{-8}$
		IgG-NCS	$0.96 \pm 0.06 \times 10^6$	$4.37 \pm 0.90 \times 10^{-4}$	$4.52 \pm 0.79 \times 10^{-10}$
V2-02	mVEGFR2	scFv	$7.94 \pm 1.24 \times 10^4$	$4.28 \pm 3.23 \times 10^{-4}$	$5.07 \pm 3.05 \times 10^{-9}$
(low-internalizing)		dscFv	$8.94 \pm 2.55 \times 10^5$	$5.57 \pm 1.25 \times 10^{-4}$	$6.60 \pm 2.39 \times 10^{-10}$
		IgG	$1.13 \pm 0.22 \times 10^6$	$3.25 \pm 1.10 \times 10^{-4}$	$2.90 \pm 0.98 \times 10^{-10}$
		scFv-PSIF	$9.84 \pm 1.52 \times 10^4$	$5.75 \pm 2.05 \times 10^{-3}$	$5.81 \pm 1.93 \times 10^{-8}$
		IgG-NCS	$1.08 \pm 0.08 \times 10^6$	$5.25 \pm 1.58 \times 10^{-4}$	$4.85 \pm 1.30 \times 10^{-10}$

Binding kinetics were analyzed against mRobo4 (R4-13i and R4-16) or mVEGFR2 (V2-05i and V2-02). Values are shown as means ± SD from three different preparations.

k_a, association rate constant ($M^{-1}s^{-1}$); k_d, dissociation rate constant (s^{-1}); K_D, equilibrium dissociation constant (k_d/k_a) (M).

mVEGFR2, but not to hVEGFR2. We also confirmed using competitive ELISA that the mAbs did not share their antigen-binding epitopes (supplemental Figure 2).

Characterization of mAbs

We purified scFvs, dimerized scFvs (dscFvs), IgGs, and scFv-PSIF as recombinant proteins. IgGs conjugated with neocarzinostatin (IgG-NCSes) were also prepared for in vivo experiments. NCSes were confirmed to be conjugated to IgG molecules in the purified IgG-NCS fraction, and the efficiencies of the NCS modifications were similar in all IgG-NCSes (1.6~1.8 NCSes per single IgG). Surface plasmon resonance analysis revealed that cell-internalizing mAbs and low-internalizing mAbs had similar affinities against antigens in all antibody forms (Table 1).

To quantify the internalization, flow cytometry analysis was performed with Cy5.5-labeled mAbs ($scFv^{Cy5.5}$, $dscFv^{Cy5.5}$, and $IgG^{Cy5.5}$; Figure 3A,C). After $mAbs^{Cy5.5}$ bound to the cell surface, internalization was induced by incubation at 37°C for 2 hours. By removing cell-surface $mAbs^{Cy5.5}$ with trypsinization, the internalized $mAbs^{Cy5.5}$ were quantified by flow cytometry. At 2 hours, approximately 30% of cell-internalizing mAbs remained after trypsinization, whereas most of the low-internalizing mAbs were degraded (Figure 3A,C). This result clearly suggested that the internalization efficiencies differed between cell-internalizing mAbs and low-internalizing mAbs, even among the three different mAb forms. In a similar manner, a time-shift analysis revealed that >40% of cell-internalizing mAbs were internalized after 8 hours of incubation (Figure 3B,D). These findings indicate that only cell-internalizing mAbs were efficiently internalized into the cells, although low-internalizing mAbs had affinities similar to those of cell-internalizing mAbs (Table 1).

Intracellular localization

The intracellular behaviors of cell-internalizing mAbs were analyzed with a confocal laser-scanning microscope. In MS1 cells, intracellular fluorescence derived from $scFv^{Cy5.5}$ was observed with cell-internalizing scFvs, but not with low-internalizing scFvs (supplemental Figure 3A,D,E,H). Fluorescence was suppressed, however, under the inhibition of energy-dependent endocytosis (supplemental Figure 3B-C,F-G). These results suggested that cell-internalizing scFvs entered into the cells via energy-dependent endocytosis.

For in-depth analysis of the intracellular behavior, confocal laser-scanning microscope analysis was performed with immunostaining of endosome markers (supplemental Figure 3Iab). After $scFvs^{Cy5.5}$ were bound to the cell-surface, the cells were incubated for an additional 1 to 8 hours at 37°C. The early endosome marker, early endosome antigen 1 (EEA1), and the late endosome marker, lysosomal-associated membrane protein 1 (LAMP1), were visualized using Alexa488-conjugated antibodies. Colocalization with EEA1+ early endosomes decreased over time (supplemental Figure 3I-M,S-W), whereas colocalization with LAMP1+ late endosomes increased (supplemental Figure 3N-R,Xab). These findings suggested that cell-internalizing scFvs were encapsulated in EEA1+ early endosomes at an early stage and eventually accumulated in LAMP1+ late endosomes. This is thought to be a typical endocytotic molecular sorting pathway.[39]

Influence of cell-internalizing activity on biodistribution

To assess the biodistribution of cell-internalizing mAbs, ^{125}I-labeled dscFvs ($dscFv^{125I}$) were intravenously injected into B16BL6 tumor-bearing mice. In this experiment, we selected the dscFv form because dscFv has superior in vivo tumor-targeting potency compared with scFv.[40] At 2 hours, the tumor distribution of anti-Robo4 and anti-VEGFR2 $dscFvs^{125I}$ was similar to but significantly higher than that of a negative control $dscFv^{125I}$ (anti-His[dscFv]^{125I}; Figure 4A-B). This finding suggested that the anti-Robo4 and anti-VEGFR2 dscFvs had tumor-targeting properties. Anti-Robo4 $dscFvs^{125I}$ also accumulated in the kidney, indicating a nonspecific distribution of dscFvs for their elimination,[41,42] because no significant difference was observed between anti-Robo4 $dscFvs^{125I}$

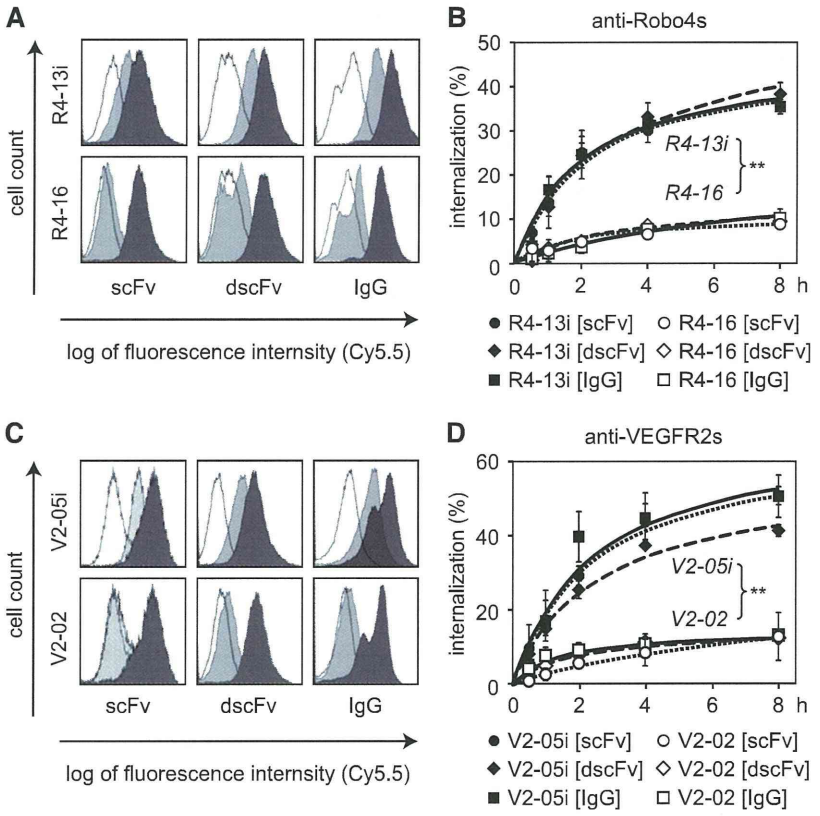

Figure 3. Cell internalization analyzed by flow cytometry. (A,C) Trypsinization to quantify internalized mAbs. Different forms of $mAbs^{Cy5.5}$ bound to the MS1 cells at 4°C. After washing out the unbound mAbs, internalization was induced for 2 hours at 37°C. To detect only internalized mAbs, cell surface proteins were trypsinized. The remaining cellular fluorescence was then analyzed by flow cytometry. (A) Anti-Robo4 $mAbs^{Cy5.5}$, (C) Anti-VEGFR2 $mAbs^{Cy5.5}$. Black, nontrypsinized group; gray, trypsinized group; white, negative control (anti-His[scFv]$^{Cy5.5}$, anti-His[dscFv]$^{Cy5.5}$, or anti-FLAG [IgG]$^{Cy5.5}$). (B,D) Time course of the internalization. After binding at 4°C, internalization was induced for 0.5, 1, 2, 4, or 8 hours at 37°C. The ratio of internalization was calculated using the following formula: internalization (%) = {internalized mAb}/{total bound mAb} × 100 (%) = {(MFI of $mAb)_T$ – (MFI of negative $control)_T$}/{(MFI of $mAb)_N$ – (MFI of negative $control)_N$} × 100 (%). T, trypsinized group; N, nontrypsinized group; MFI, mean fluorescence intensity. (B) Closed and open markers indicate R4-13i and R4-16, respectively. (D) Closed and open markers indicate V2-05i and V2-02, respectively. (B,D) Circles, diamonds, and squares indicate scFv, dscFv, and IgG, respectively. Each experiment was performed in triplicate. Values are shown as means ± SD. $^{**}P < .01$; internalizing mAb versus low-internalizing mAb in each form by 2-way ANOVA (n = 3).

and anti-His[dscFv]^{125I} (Figure 4A). Importantly, the accumulation of anti-VEGFR2 $dscFvs^{125I}$ in the kidney was significantly greater than that of anti-His[dscFv]^{125I} (Figure 4B). A similar accumulation of anti-VEGFR2 $dscFvs^{125I}$, but not anti-Robo4 $dscFvs^{125I}$ (Figure 4A), was observed in the heart (Figure 4B).

To confirm this phenomenon, the localization of dscFvs in the tissues was analyzed by immunofluorescence studies (Figure 4E-S). Biotin-labeled dscFvs ($dscFvs^{Bio}$) were intravenously administered to B16BL6 tumor–bearing mice and the tumors, kidneys, and hearts were extracted 2 hours after injection. The $dscFv^{Bio}$ and vascular endothelial cells were stained by streptavidin-AP and anti-CD31 antibody, respectively. In the tumor sections, all of the anti-Robo4 and anti-VEGFR2 $dscFvs^{Bio}$ were clearly detected with CD31+ tumor blood vasculature, whereas anti-His[dscFv]^{Bio} was not detectable (Figure 4E,H,K,N,Q). This finding suggested that both anti-Robo4 and anti-VEGFR2 dscFvs recognized tumor endothelial cells in vivo, which contributed to their accumulation in the tumor. Interestingly, in the kidney and heart sections, signals around CD31+ blood vasculature were detectable only with the anti-VEGFR2 $dscFvs^{Bio}$, and not with anti-Robo4 $dscFvs^{Bio}$ or anti-His[dscFv]^{Bio} (Figure 4F-G,I-J,L-M,O-P,R-S). This finding was compatible with the biodistribution results (Figure 4A-B), which suggested that anti-VEGFR2 dscFvs recognized VEGFR2 on normal blood vessels because VEGFR2 plays an important role in normal tissues, including the kidney and heart.[31-33] No specific accumulation of anti-Robo4 dscFvs was observed in normal tissues, suggesting that the anti-Robo4 mAbs were useful for specific tumor vascular targeting.

Comparison of the cell-internalizing mAbs and low-internalizing mAbs revealed a significantly greater accumulation of cell-internalizing $dscFvs^{125I}$ in the tumors compared with low-internalizing $dscFvs^{125I}$ at 24 hours (Figure 4C-D), whereas no differences were observed at 2 hours (Figure 4A-B). This finding suggested that cell-internalizing mAbs were retained in the tumor for a longer time than the low-internalizing mAbs. This phenomenon was also observed in the kidney and heart with the anti-VEGFR2 dscFvs (Figure 4D). This retention might be caused by the mAb internalization, which allowed the mAb to escape from the bloodstream and accumulate in the tumor blood endothelial cells. Taken together, these results suggest that mAb internalization into the tumor endothelium improves mAb-based drug-delivery in vivo.

Enhanced antitumor effect depends on the cell-internalizing activity

To assess the antitumor potencies of the cell-internalizing mAbs, we selected the scFv-PSIF and IgG-NCS forms. Both forms were suitable models of ADCs because both drugs are used clinically as successful anticancer medicines.[10,43] First, the in vitro cell-killing activities of scFv-PSIFs and IgG-NCSes were estimated by a cytotoxicity assay with MS1 cells (Figure 5A-D). Both forms of cell-internalizing mAbs showed an approximately 10-fold higher cytotoxicity than the low-internalizing mAbs. These findings clearly suggest that internalization enhanced the delivery of conjugated drugs into the cells because our cell-internalizing mAbs and low-internalizing mAbs had similar affinities against antigens (Table 1).

As the therapy experiment in vivo, scFv-PSIFs and IgG-NCSes were intravenously injected into B16BL6 tumor–bearing mice once every 2 days for a total of 5 injections (Figure 5E-H). All cell-internalizing mAbs significantly suppressed tumor growth, whereas the antitumor effects of the low-internalizing antibodies were

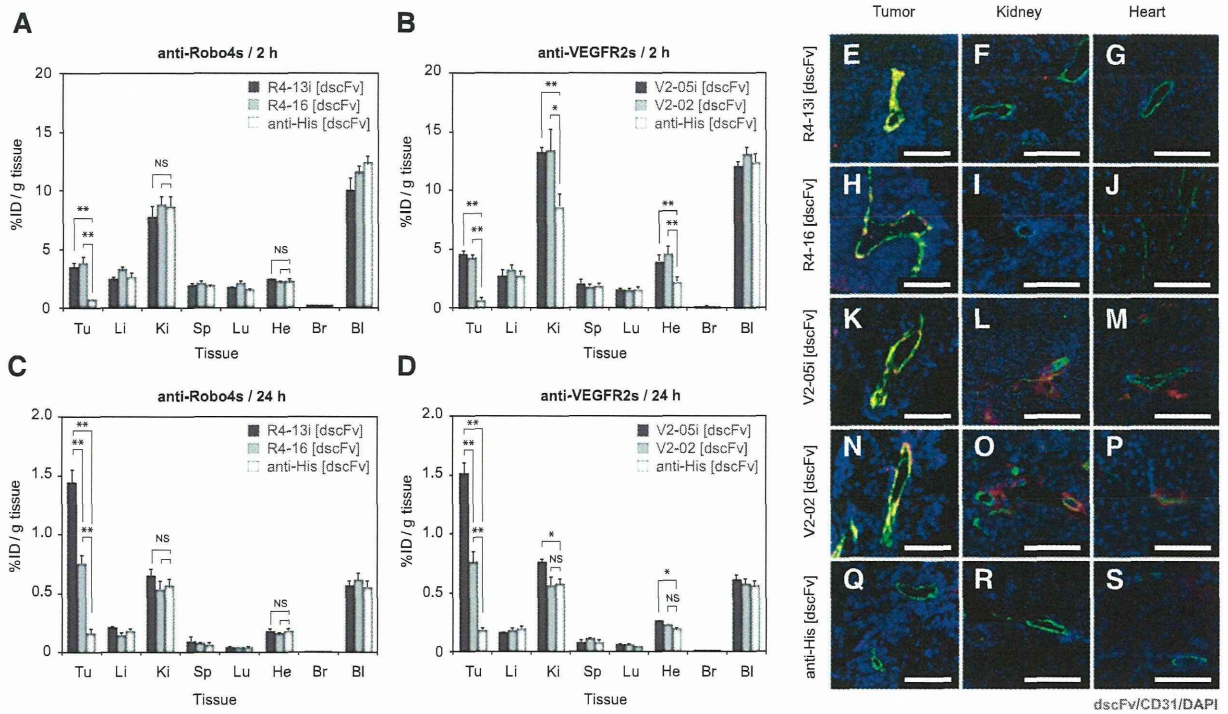

Figure 4. In vivo tumor-targeting activity of cell-internalizing mAbs. (A-D) Biodistribution of dscFvs in B16BL6 tumor–bearing mice. B16BL6 tumor–bearing mice were intravenously administered with anti-Robo4 dscFvs^{125I} (A,C) or anti-VEGFR2 dscFvs^{125I} (B,D). Each organ was extracted after 2 hours (A,B) or 24 hours (C,D), and the radioactivity was measured using a γ counter. %ID/g tissue was calculated using the following formula: %ID/g tissue = (count/g tissue)/(total injected count) × 100 (%). Tu, tumor; Li, liver; Ki, kidney; Sp, spleen; Lu, lung; He, heart; Br, brain; Bl, blood. (A,C) black; R4-13i[dscFv]^{125I}; gray, R4-16[dscFv]^{125I}; white, anti-His[dscFv]^{125I}. (B,D) black, V2-05i[dscFv]^{125I}; gray, V2-02[dscFv]^{125I}; white, anti-His[dscFv]^{125I}. Values are shown as means ± SEM. $^*P < .05$; $^{**}P < 0.01$; NS, not significant in Student's *t*-test (n = 11). (E-S) Co-immunostaining of dscFvs with CD31$^+$ blood endothelial cells on the tissue section. B16BL6 tumor–bearing mice were intravenously administered dscFvs^{Bio}. The tumor, kidney, and heart were extracted after 2 hours. Tissue sections of tumor, kidney, and heart were stained with streptavidin-PE conjugate. The blood vasculature was also stained with anti-CD31 antibody. Images were digitally merged. Red, dscFv^{Bio}; green, CD31; blue, DAPI (nucleus); yellow, colocalized region of red and green. Scale bar represents 100 μm. (E-G) R4-13i[dscFv]; (H-J) R4-16[dscFv]; (K-M) V2-05i[dscFv]; (N-P) V2-02[dscFv]; (Q-S) anti-His[dscFv]. (E,H,K,N,Q) Tumor section, (F,I,L,O,R) kidney section, and (G,J,M,P,S) heart section.

similar to those of the negative controls (anti-His[scFv]-PSIF and anti-FLAG[IgG]-NCS). The antitumor effects of R4-13i and V2-05i were similar in both ADC forms. These findings strongly suggest that the cell-internalizing activity of the mAbs was essential to maximize the delivery of the conjugated drug into the target cells, which significantly enhanced the antitumor effect of the ADCs.

Interestingly, the group of mice administered V2-05i[scFv]-PSIF had a significant loss of body weight, whereas the other groups did not (Figure 5I-L). As a preliminary result, 6 of 7 mice died in the V2-05i[scFv]-PSIF group with a similar protocol but with a fourfold higher dosage (60 pmol/mouse), perhaps because of the disruption of VEGFR2-positive cells in normal tissues by V2-05i[scFv]-PSIF, as shown in Figure 4. This side effect was not observed in the V2-05i [IgG]-NCS group. Therefore, we also hypothesized that the toxicity of NCS in normal cells was weak because NCS inhibits DNA synthesis in growing cells, such as tumor cells.[44] At a higher dosage, however, V2-05i[IgG]-NCS carries the risk of side effects. With regard to this point, none of the anti-Robo4 ADCs induced a loss of body weight; therefore, we concluded that Robo4 is a potential target for tumor vascular targeting with ADC.

Discussion

This study led to three novel findings. First, we demonstrated a rapid screening system for cell-internalizing mAbs in combination with the phage antibody library, which accelerated the identification of desired cell-internalizing mAbs. Second, comparative in vivo studies using cell-internalizing mAbs and low-internalizing mAbs with the same affinity values revealed that mAb internalization contributed to tumor targeting and enhanced the antitumor effects of the ADCs. Third, the first in vivo therapeutic application with anti-Robo4 mAb revealed that Robo4 is a therapeutic target on the tumor endothelial cells. The first and second findings will greatly contribute to the development of antibody therapies based on cell-internalizing antibodies such as ADCs, targeted liposomal drugs, or imaging. The third finding provides a new focus regarding the role of Robo4 biology in the body, such as the decreased side effects associated with depleting Robo4-positive endothelial cells in vivo.

This method allowed us to successfully isolate anti-Robo4 and anti-VEGFR2 cell-internalizing mAbs in combination with a phage antibody library and a PSIF-based screening system. This method provided one-step screening of cell-internalization of hundreds of "monoclonal" candidates. This is the main advantage of the present system over the old screening system, which required handling a "polyclonal" pool of mAbs.[6,7] The innovative feature of our method is the use of PSIF as a fusion partner for antibodies in scFv format, thus facilitating the identification of antibody fragments capable of efficient internalization. The scFv fusion is much easier than the chemical conjugation of the antibody to a cytotoxic drug. In principle, this method can be applied to other phage libraries, such as nonimmune phage antibody libraries[35,45] or synthetic

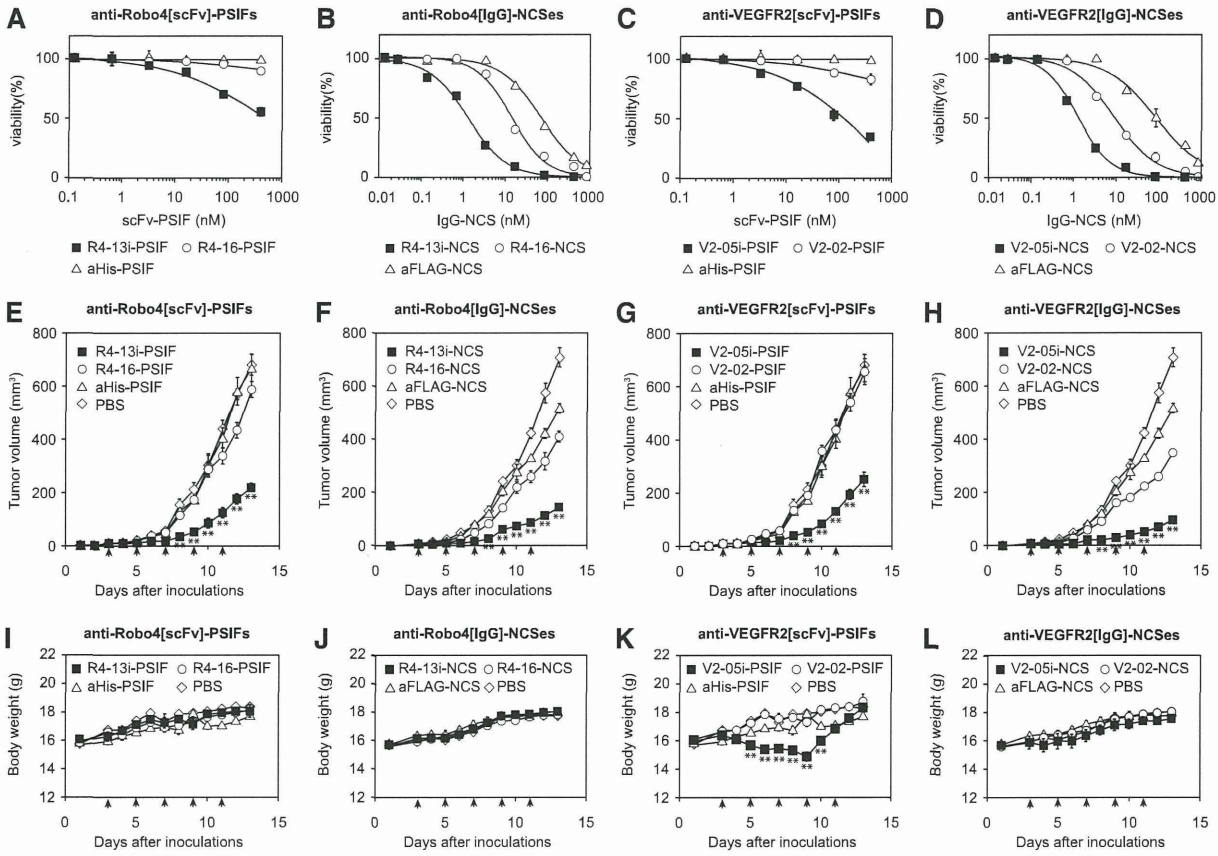

Figure 5. Enhanced anti-tumor effect of cell-internalizing mAbs. (A-D) Cytotoxicity of scFv-PSIF and IgG-NCS against MS1 cells. MS1 cells were incubated with serially diluted mAb-drug conjugates for 24 hours. Cell viability was then measured using a WST-8 assay. Closed square, internalizing mAbs; open circle, low-internalizing mAbs; open triangle, negative controls. (A) anti-Robo4[scFv]-PSIFs, (B) anti-Robo4[IgG]-NCSes, (C) anti-VEGFR2[scFv]-PSIFs, (D) anti-VEGFR2[IgG]-NCSes. Anti-His[scFv]-PSIF and anti-FLAG[IgG]-NCS were used as negative controls. Values are shown as means ± SD. (E-H) Antitumor effects of scFv-PSIFs or IgG-NCSes. B16BL6 cells were inoculated intracutaneously into C57BL6 mice on day 0. On days 3, 5, 7, 9, and 11, mAb-drug conjugates were intravenously administered *(arrow heads)*. Tumor volume was calculated using the following formula: tumor volume (mm^3) = {major axis of tumor (mm)} × {minor axis of tumor (mm)}^{2} × 0.4. Closed square, internalizing mAbs; open circle, low-internalizing mAbs; open triangle, negative controls (anti-His[scFv]-PSIF or anti-FLAG[IgG]-NCS); open diamond, PBS. (E) Anti-Robo4[scFv]-PSIFs, (F) anti-Robo4[IgG]-NCSes, (G) anti-VEGFR2[scFv]-PSIFs, (H) anti-VEGFR2[IgG]-NCSes. Values are shown as means ± SEM. $^{**}P < 0.01$; internalizing mAbs versus low-internalizing mAbs by Bonferroni post hoc analysis with two-way ANOVA (n = 6). (I-L) Change in body weight during therapy experiment. Closed square, internalizing mAbs; open circle, low-internalizing mAbs; open triangle, negative controls (anti-His[scFv]-PSIF or anti-FLAG[IgG]-NCS); open diamond, PBS. (I) anti-Robo4[scFv]-PSIFs, (J) anti-Robo4[IgG]-NCSes, (K) anti-VEGFR2[scFv]-PSIFs, (L) anti-VEGFR2[IgG]-NCSes. Values are shown as means ± SEM. $^{**}P < 0.01$; internalizing mAbs versus PBS by Bonferroni post hoc analysis with two-way ANOVA (n = 6).

human phage antibody libraries,[46,47] which have already been developed. This system can expand the versatility of phage display systems, which will thus contribute to the development of other cell-internalizing antibodies against various types of antigens for effective cancer therapy.

A comparison of cell-internalizing mAbs with low-internalizing mAbs revealed the strength of the cell-internalizing mAbs in terms of the biodistribution and therapeutic effects. Until now, how internalization contributes to the biodistribution of mAbs has been unclear. In this report, we could use a comparative study to clarify this question because we produced both cell-internalizing mAbs and low-internalizing mAbs with similar binding affinities. As a result, more cell-internalizing mAbs than low-internalizing mAbs were significantly accumulated in the tumor. This is the first evidence to support that mAbs with high internalization activity have greater tumor-targeting potency. This information is also useful for other applications that benefit from cell-internalizing mAbs, such as liposomal drugs, bioactive proteins/peptides, and viral vectors.[48,49]

Until now, the usefulness of Robo4-targeted therapy has not been established. Therapy to target VEGF-VEGFR signaling is already common, but the risk of side effects must be addressed.[31-33] Although VEGFR expression is upregulated on tumor vessels, it is also observed on the endothelium in healthy tissues. Previous reports also mentioned the toxicity associated with the anti-VEGFR therapies in mouse models[50] and the clinical trial.[51] Therefore, alternative therapies that target tumor angiogenesis are desired. In the present study, we revealed the possibility that anti-Robo4 ADCs were safer than anti-VEGFR2 ADCs, although they had similar antitumor effects. The findings from immunofluorescence and biodistribution studies also support the notion that anti-Robo4 mAbs could accumulate in the tumor without distributing to normal tissues. This is the first finding of Robo4-targeted therapy and suggests that Robo4 is a potential alternative target for tumor vascular targeting. Of course, additional experiments are needed to establish anti-Robo4 as a novel tool in tumor vascular targeting. For example, the pathological observations of normal blood vessels, in-depth toxicological analysis,

or the efficacy against other clinical relevant tumor models, are important for the successful story. Such basic analyses regarding Robo4 might accelerate the development of novel medicines that target tumor angiogenesis, including anti-Robo4 ADCs.

Acknowledgments

This study was supported by Grant-in-Aid for Scientific research (B) and Grant-in-Aid for Scientific Research on Innovative Areas from the Ministry of Education, Culture, Sports, Science, and Technology of Japan and the Japan Society for the Promotion of Science; Strategic Japanese-Swiss Cooperative Program from Japan Science and Technology Agency (JST) and the Swiss Federal Institute of Technology Zurich.

Authorship

Contribution: Y.M. designed the study; M.Y. and Y. Tsumori performed the experiments; Y.M. and M.Y. analyzed the data; Y.M. and M.Y. wrote the initial manuscript; S.T. and Y. Tsutsumi contributed to the phage display; Y.Y. and N.O. contributed to animal experiments; Y.O., W.C.A., and T.D. contributed to Robo4 related analysis; Y.M. and S.N. were responsible for the overall project. All authors edited the manuscript.

Conflict-of-interest disclosure: The authors declare no competing financial interests.

Correspondence: Yohei Mukai and Shinsaku Nakagawa, Laboratory of Biotechnology and Therapeutics, Graduate School of Pharmaceutical Sciences, Osaka University, 1–6 Yamadaoka, Suita, Osaka 565–0871, Japan; e-mail: y-mukai@nibio.go.jp and nakagawa@phs.osaka-u.ac.jp.

References

1. Alley SC, Okeley NM, Senter PD. Antibody-drug conjugates: targeted drug delivery for cancer. *Curr Opin Chem Biol.* 2010;14(4):529-537.
2. Isakoff SJ, Baselga J. Trastuzumab-DM1: building a chemotherapy-free road in the treatment of human epidermal growth factor receptor 2-positive breast cancer. *J Clin Oncol.* 2011;29(4): 351-354.
3. Ansell SM. Brentuximab vedotin: delivering an antimitotic drug to activated lymphoma cells. *Expert Opin Investig Drugs.* 2011;20(1):99-105.
4. Reichert JM. Antibody-based therapeutics to watch in 2011. *MAbs.* 2011;3(1):76-99.
5. Gerber HP, Senter PD, Grewal IS. Antibody drug-conjugates targeting the tumor vasculature: Current and future developments. *MAbs.* 2009; 1(3):247-253.
6. Poul MA, Becerril B, Nielsen UB, et al. Selection of tumor-specific internalizing human antibodies from phage libraries. *J Mol Biol.* 2000;301(5): 1149-1161.
7. An F, Drummond DC, Wilson S, et al. Targeted drug delivery to mesothelioma cells using functionally selected internalizing human single-chain antibodies. *Mol Cancer Ther.* 2008;7(3): 569-578.
8. Mukai Y, Sugita T, Yamato T, et al. Creation of novel Protein Transduction Domain (PTD) mutants by a phage display-based high-throughput screening system. *Biol Pharm Bull.* 2006;29(8):1570-1574.
9. Chaudhary VK, FitzGerald DJ, Adhya S, et al. Activity of a recombinant fusion protein between transforming growth factor type alpha and Pseudomonas toxin. *Proc Natl Acad Sci USA.* 1987;84(13):4538-4542.
10. Kreitman RJ, Wilson WH, Bergeron K, et al. Efficacy of the anti-CD22 recombinant immunotoxin BL22 in chemotherapy-resistant hairy-cell leukemia. *N Engl J Med.* 2001;345(4): 241-247.
11. Pastan I, FitzGerald D. Pseudomonas exotoxin: chimeric toxins. *J Biol Chem.* 1989;264(26): 15157-15160.
12. Legg JA, Herbert JMJ, Clissold P, et al. Slits and Roundabouts in cancer, tumour angiogenesis and endothelial cell migration. *Angiogenesis.* 2008; 11(1):13-21.
13. Huminiecki L, Bicknell R. In silico cloning of novel endothelial-specific genes. *Genome Res.* 2000; 10(11):1796-1806.
14. Huminiecki L, Gorn M, Suchting S, et al. Magic roundabout is a new member of the roundabout receptor family that is endothelial specific and expressed at sites of active angiogenesis. *Genomics.* 2002;79(4):547-552.
15. Smith-Berdan S, Nguyen A, Hassanein D, et al. Robo4 cooperates with CXCR4 to specify hematopoietic stem cell localization to bone marrow niches. *Cell Stem Cell.* 2011;8(1):72-83.
16. Park KW, Morrison CM, Sorensen LK, et al. Robo4 is a vascular-specific receptor that inhibits endothelial migration. *Dev Biol.* 2003;261(1): 251-267.
17. Seth P, Lin Y, Hanai J, et al. Magic roundabout, a tumor endothelial marker: expression and signaling. *Biochem Biophys Res Commun.* 2005; 332(2):533-541.
18. Okada Y, Yano K, Jin E, et al. A three-kilobase fragment of the human Robo4 promoter directs cell type-specific expression in endothelium. *Circ Res.* 2007;100(12):1712-1722.
19. Okada Y, Jin E, Nikolova-Krstevski V, et al. A GABP-binding element in the Robo4 promoter is necessary for endothelial expression in vivo. *Blood.* 2008;112(6):2336-2339.
20. Jones CA, London NR, Chen H, et al. Robo4 stabilizes the vascular network by inhibiting pathologic angiogenesis and endothelial hyperpermeability. *Nat Med.* 2008;14(4):448-453.
21. Jones CA, Nishiya N, London NR, et al. Slit2-Robo4 signalling promotes vascular stability by blocking Arf6 activity. *Nat Cell Biol.* 2009; 11(11):1325-1331.
22. Marlow R, Binnewies M, Sorensen LK, et al. Vascular Robo4 restricts proangiogenic VEGF signaling in breast. *Proc Natl Acad Sci USA.* 2010;107(23):10520-10525.
23. Koch AW, Mathivet T, Larrivée B, et al. Robo4 maintains vessel integrity and inhibits angiogenesis by interacting with UNC5B. *Dev Cell.* 2011;20(1):33-46.
24. Kerbel RS. Tumor angiogenesis. *N Engl J Med.* 2008;358(19):2039-2049.
25. Paleolog EM. Angiogenesis in rheumatoid arthritis. *Arthritis Res.* 2002;4(Suppl 3):S81-S90.
26. Tonnesen MG, Feng X, Clark RA. Angiogenesis in wound healing. *J Investig Dermatol Symp Proc.* 2000;5(1):40-46.
27. Olsson AK, Dimberg A, Kreuger J, et al. VEGF receptor signalling - in control of vascular function. *Nat Rev Mol Cell Biol.* 2006;7(5):359-371.
28. Crawford Y, Ferrara N. VEGF inhibition: insights from preclinical and clinical studies. *Cell Tissue Res.* 2009;335(1):261-269.
29. Wicki A, Rochlitz C, Orleth A, et al. Targeting tumor-associated endothelial cells: anti-VEGFR2 immunoliposomes mediate tumor vessel disruption and inhibit tumor growth. *Clin Cancer Res.* 2012;18(2):454-464.
30. Witmer AN, Dai J, Weich HA, et al. Expression of vascular endothelial growth factor receptors 1, 2, and 3 in quiescent endothelia. *J Histochem Cytochem.* 2002;50(6):767-777.
31. Kamba T, McDonald DM. Mechanisms of adverse effects of anti-VEGF therapy for cancer. *Br J Cancer.* 2007;96(12):1788-1795.
32. Eremina V, Jefferson JA, Kowalewska J, et al. VEGF inhibition and renal thrombotic microangiopathy. *N Engl J Med.* 2008;358(11):1129-1136.
33. Choueiri TK, Mayer EL, Je Y, et al. Congestive heart failure risk in patients with breast cancer treated with bevacizumab. *J Clin Oncol.* 2011; 29(6):632-638.
34. Yoshikawa M, Mukai Y, Okada Y, et al. Ligand-independent assembly of purified soluble magic roundabout (Robo4), a tumor-specific endothelial marker. *Protein Expr Purif.* 2008;61(1):78-82.
35. Imai S, Mukai Y, Nagano K, et al. Quality enhancement of the non-immune phage scFv library to isolate effective antibodies. *Biol Pharm Bull.* 2006;29(7):1325-1330.
36. Yoshikawa M, Mukai Y, Tsunoda S, et al. Modifying the antigen-immunization schedule improves the variety of monoclonal antibodies obtained from immune-phage antibody libraries against HIV-1 Nef and Vif. *J Biosci Bioeng.* 2011; 111(5):597-599.
37. Yamamoto Y, Tsutsumi Y, Yoshioka Y, et al. Site-specific PEGylation of a lysine-deficient TNF-alpha with full bioactivity. *Nat Biotechnol.* 2003;21(5):546-552.
38. Hunter WM, Greenwood FC. Preparation of iodine-131 labelled human growth hormone of high specific activity. *Nature.* 1962;194:495-496.
39. Mellman I. Endocytosis and molecular sorting. *Annu Rev Cell Dev Biol.* 1996;12:575-625.
40. Holliger P, Hudson PJ. Engineered antibody fragments and the rise of single domains. *Nat Biotechnol.* 2005;23(9):1126-1136.
41. Pavlinkova G, Beresford GW, Booth BJ, et al. Pharmacokinetics and biodistribution of engineered single-chain antibody constructs of MAb CC49 in colon carcinoma xenografts. *J Nucl Med.* 1999;40(9):1536-1546.
42. Schneider DW, Heitner T, Alicke B, et al. In vivo biodistribution, PET imaging, and tumor accumulation of 86Y- and 111In-antimindin/RG-1,

engineered antibody fragments in LNCaP tumor-bearing nude mice. *J Nucl Med.* 2009; 50(3):435-443.

43. Maeda H. SMANCS and polymer-conjugated macromolecular drugs: advantages in cancer chemotherapy. *Adv Drug Deliv Rev.* 2001;46(1-3): 169-185.
44. Kappen LS, Goldberg IH. Activation and inactivation of neocarzinostatin-induced cleavage of DNA. *Nucleic Acids Res.* 1978; 5(8):2959-2967.
45. Okamoto T, Mukai Y, Yoshioka Y, et al. Optimal construction of non-immune scFv phage display libraries from mouse bone marrow and spleen established to select specific scFvs efficiently binding to antigen. *Biochem Biophys Res Commun.* 2004;323(2): 583-591.
46. Silacci M, Brack S, Schirru G, et al. Design, construction, and characterization of a large synthetic human antibody phage display library. *Proteomics.* 2005;5(9): 2340-2350.
47. Villa A, Lovato V, Bujak E, et al. A novel synthetic naïve human antibody library allows the isolation of antibodies against a new epitope of oncofetal fibronectin. *MAbs.* 2011; 3(3):264-272.
48. Sapra P, Allen TM. Internalizing antibodies are necessary for improved therapeutic efficacy of antibody-targeted liposomal drugs. *Cancer Res.* 2002;62(24):7190-7194.
49. Pastan I, Hassan R, Fitzgerald DJ, et al. Immunotoxin therapy of cancer. *Nat Rev Cancer.* 2006;6(7):559-565.
50. Chinnasamy D, Yu Z, Theoret MR, et al. Gene therapy using genetically modified lymphocytes targeting VEGFR-2 inhibits the growth of vascularized syngenic tumors in mice. *J Clin Invest.* 2010;120(11):3953-3968.
51. Nagayama H, Matsumoto K, Isoo N, et al. Gastrointestinal bleeding during anti-angiogenic peptide vaccination in combination with gemcitabine for advanced pancreatic cancer. *Clin J Gastroenterol.* 2010;3(6):307-317.

J Nanopart Res (2013) 15:1305
DOI 10.1007/s11051-012-1305-7

TECHNOLOGY AND APPLICATIONS

Design of Au/SPIO composite nanoparticle for facile and biocompatible surface functionalization via Au–S bond

Satoshi Seino · Yujin Shibata · Masayuki Yamanaka · Takashi Nakagawa · Yohei Mukai · Shinsaku Nakagawa · Takao A. Yamamoto

Received: 29 June 2012 / Accepted: 10 November 2012 / Published online: 5 December 2012

Abstract Immobilization of Au nanoparticles on super-paramagnetic iron-oxide (SPIO) enables facile and biocompatible surface functionalization via Au–S bond. Au/SPIO composite nanoparticle is easily modified by thiol-modified polyethylene glycol (PEG-SH), and they are successfully applied on MR tumor imaging. However, its large hydrodynamic size ($\sim$150 nm) still causes the accumulation to liver in vivo. In this study, we controlled the hydrodynamic size of Au/SPIO by testing different raw SPIOs and stabilizing polymers. As the best candidate, Au/Molday-ION which was synthesized from Molday-ION and polyvinyl alcohol comprised the hydrodynamic size of 56 nm. Moreover, PEGylated Au/Molday-ION showed excellent dispersibility in blood serum, with the hydrodynamic size of 65 nm. This surface functionalization strategy is effective for the constructions of magnetic nanocarriers for in vivo applications.

S. Seino (✉) · Y. Shibata · M. Yamanaka · T. Nakagawa · T. A. Yamamoto
Graduate School of Engineering, Osaka University, 2-1 Yamadaoka, Suita 565-0871, Japan
e-mail: seino@mit.eng.osaka-u.ac.jp

Y. Mukai · S. Nakagawa
Graduate School of Pharmaceutical Sciences and Center for Advanced Medical Engineering and Informatics, Osaka University, 1-6 Yamadaoka, Suita, Osaka 565-0871, Japan

Keywords Au · Composite nanoparticle · Polyethylene glycol · Radiochemical process · SPIO

Introduction

In recent years, in vivo applications of nanoparticle materials are extensively investigated for the realization of advanced medical treatments such as drug delivery system, gene therapy, and so on (Allen and Cullis 2004; Balmayor et al. 2011). Especially, iron-oxide nanoparticles are paid much attention because of their attractive magnetic properties and biocompatibilities (Gupta and Gupta 2005; Mornet et al. 2004; Neuberger et al. 2005). For in vivo uses, super paramagnetic iron oxide (SPIO) is usually applied because of its size-dependent magnetic property. The SPIOs decrease the signal intensity on T_2-weighted MR images and is clinically used for diagnosing liver cancer (Mitchell 1999). Typical examples are Feridex (AMAG Pharmaceuticals, Inc., MA) and Resovist (Bayer Schering Pharma AG., Germany), both of which contain a core iron-oxide nanoparticle coated with a dextran polymer (Weinstein et al. 2010). When injected into the blood stream, the SPIOs are avidly taken up by phagocytic cells, such as the Kupffer cell fraction of the liver, which enables the MRI diagnosis of liver cancer (Weinstein et al. 2010).